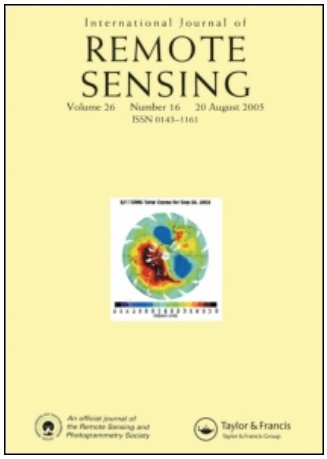


International Journal of Remote Sensing
Publication details, including instructions for authors and subscription information:
http://www.informaworld.com/smpp/title~content=t713722504

# Estimating tree crown size with spatial information of high resolution optical remotely sensed imagery

Online Publication Date: 01 January 2007
To cite this Article: Song, C. (2007) 'Estimating tree crown size with spatial information of high resolution optical remotely sensed imagery', International Journal of Remote Sensing, 28:15, 3305 - 3322
To link to this article: DOI: 10.1080/01431160600993413
URL: http://dx.doi.org/10.1080/01431160600993413

*International Journal of Remote Sensing*
Vol. 28, No. 15, 10 August 2007, 3305–3322





# Estimating tree crown size with spatial information of high resolution optical remotely sensed imagery

C. SONG*
Department of Geography, CB No. 3220, 205 Saunders Hall, University of North Carolina at Chapel Hill, Chapel Hill, NC 27599, USA

(*Received 24 January 2006; in final form 3 September 2006*)

Tree crown size is a critical biophysical parameter that influences carbon, water and energy exchanges between forest ecosystems and the atmosphere. This study explores the potential of using spatial information of high resolution optical imagery in estimating mean tree crown diameter on a stand basis with an Ikonos image in the Blackwood Division of Duke Forest and its surrounding areas. The theory is based on the disc scene model that the ratio of image variances at two spatial resolutions is determined by the scene structure only. The mean tree crown diameter of a stand on the ground was estimated with a circular sampling plot made in the middle of the stand. The stands were then delineated in the panchromatic band of the Ikonos image. The relationship between mean tree crown diameter with image variance at a single spatial resolution, the ratio of image variances at two spatial resolutions, and the difference of image variances at two spatial resolutions were studied for conifer and hardwood stands, respectively. It was found that the ratio of image variances at 2 m and 3 m spatial resolutions best estimate conifer tree crown diameter ($R^2$=0.7282). Though the image variance at a single resolution and the difference of image variances at two spatial resolutions are also significantly correlated to conifer tree crown diameter, the $R^2$ is lower. Due to the continuity in canopy structure, the approach does not work well for hardwood stands.

## 1. Introduction

Tree crown size is a critical biophysical parameter of forest canopy because it influences the rate of carbon, water and energy exchanges between forest ecosystems and the atmosphere. The size of the crown is not only a critical factor determining the surface roughness of forest canopies, but also relates to rooting depth based on the pipe theory (Shinozaki *et al.* 1964), all of which in turn strongly influences gaseous and water exchanges between forest ecosystems and the atmosphere (Betts *et al.* 1997). Tree crowns are the major spatial scale at which the leaves clump in the canopy (Kucharik *et al.* 1999), and determine the amount of shaded and sunlit leaves within a canopy (Li and Strahler 1992). Thus, the crown size of a stand is also a critical input parameter to numerous models that simulate energy and/or mass transfer through the canopy (Chen and Coughenour 1994, Li *et al.* 1995, Ni *et al.* 1997, Song and Band 2004). In addition, tree crown diameter has been found to be closely related to tree bole diameter (Bechtold 2004, Hemery *et al.* 2005), and thus can further be used to study forest biomass (Alves and Santos 2002). However, tree

*Email: csong@email.unc.edu

*International Journal of Remote Sensing*
ISSN 0143-1161 print/ISSN 1366-5901 online 
http://www.tandf.co.uk/journals
DOI: 10.1080/01431160600993413

crown size data are extremely scarce because they are very laborious to obtain in the field.

Numerous studies investigated the possibility of estimating tree crown size from optical imagery. A pioneering study was the inversion of tree crown size and cover on a stand basis using the Li–Strahler model with Landsat Thematic Mapper (TM) imagery (Li and Strahler 1985). Franklin and Strahler (1988) and Wu and Strahler (1993) achieved some success in estimating tree crown size applying the Li–Strahler model. However, Woodcock *et al.* (1994, 1997) found that Li–Strahler model was effective in estimating tree cover, but separation of tree size and cover was difficult with Landsat TM imagery. In addition to the physically based models, many other studies on extracting tree crown sizes were based on image spatial properties. Though image spatial properties of airborne high spatial resolution imagery were found to be diagnostic of scene structure (Woodcock *et al.* 1988a,b, St-Onge and Cavayas 1995, 1997, Treitz and Howarth, 2000), Cohen and Spies (1990) concluded that the spatial properties of Landsat TM imagery were not very helpful in obtaining canopy structure because the pixel size is too big compared to tree crown size. Another approach of obtaining tree crown size is direct delineation of tree crowns based on airborne very high spatial resolution imagery (Pollock 1996, Culvenor 2002). But these applications are very limited due to lack of available data and spatial scope of the operations.

Recent advances in availability of high spatial resolution optical imagery from space (e.g. Ikonos and Quickbird) have further spurred the interest in obtaining detailed canopy structure from remote sensing for a wide range of applications, such as ecology (Hurtt *et al.* 2003, Clark *et al.* 2004a,b, Wulder *et al.* 2004) and forest management (Read *et al.* 2003, White *et al.* 2004, Wallace and Marsh 2005). Unlike the airborne optical imagery previously used, the space-borne satellite imagery can be obtained anywhere around the Earth. Studies continue to show that image spatial properties of the high resolution optical imagery from space are diagnostic of forest structure (Franklin *et al.* 2001, Song and Woodcock 2002, Wang *et al.* 2004). In a more rigorous study, Asner *et al.* (2002) compared tree crown size measured directly in the Ikonos image with those measured on the ground and found that the measurements from the images were biased toward large trees. Similarly, Read *et al.* (2003) found that the tree crown area measured in an Ikonos image can be directly related to tree trunk diameter on the ground. The objective of this study is to estimate tree crown size on a stand basis using spatial information of Ikonos imagery.

## 2. Methodology

### 2.1 *Study area*

The study area is located in the Blackwood Division of Duke Forest (35°58′42″ N, 79°05′39″ W) and its surrounding areas in the Piedmont region of North Carolina. The mean annual temperature is 15.5°C and the mean annual precipitation is 1140 mm for the area (Schafer *et al.* 2002). Soils are low fertility acidic Hapludalf in the Enon Series, which are typical of the south-eastern United States, with a clayey loam in the top 0.3 m and clay below to the bedrock at 0.7 m. The local terrains are relatively flat (<5% slope) (http://face.env.duke.edu/site.cfm). Vegetation over the region ranges from relatively pure conifers and hardwood stands to varying degrees of a mixture of the two. Conifer species are dominated by the Loblolly pine (*Pinus*

*taeda* L.). The hardwood stands are dominated by White Oak (*Quercus alba* L.), Red Oak (*Q. rubra* L.), Sweet Gum (*Liquidambar styraciflua* L.), Red Maple (*Acer rubrum* L.), Tulip Popular (*Liriodendron tulipifera* L.) and Hickory (*Carya ovata*).

### 2.2 *Data collection*

A remotely sensed image from the Ikonos satellite collected on 23 September 2004 is used in this study to test the algorithms estimating tree crown sizes. The centre of the image was the FACE (Free Air $CO_2$ Enrichment) site at the Blackwood Division of Duke Forest (Oren *et al.* 2001). The size of the image is 10 km × 10 km. The sun elevation and azimuth angles at the time of image acquisition were 59.0° and 159.9°, respectively. The cloud cover in the image is zero.

Fieldwork is an evolving process in this study. A total of 21 circular plots with variable diameter were made in this study during late spring and early summer of 2005 within the extent of the Ikonos image. The default size of a plot was 30 m in diameter, but the size was increased for stands at late successional stage with fewer larger trees and decreased for stands at early successional stage with many small trees. The plots were made in the middle of relatively large and uniform stands. The centre locations of the plots were recorded with a Garmin 12XL GPS receiver. After the centre of a plot was located, the plot boundary was identified with flagging tapes. All trees around the edge were clearly marked whether they were inside or outside the plot.

The diameter at breast height (DBH) was measured for each individual reaching the canopy with diameter tapes. The trees in the plots were not numbered in order to save time. After measurement of a tree, chalk marks were made on the tree trunk to avoid repeated measurements. DBH was recorded along with the species. The tree crown size was measured in two orthogonal directions with one along the maximum width with fibreglass tapes. The two crown diameter measurements were averaged to the tree crown diameter (CD). The fieldwork requires a minimum of two persons working together in the field. Measurement of tree crown size was an evolving process in this study. DBH and CD were measured for each individual for the first plot made in a Loblolly pine stand. A strong allometric relationship between DBH and CD was found as

$$\ln(CD) = b_0 + b_1 \ln(DBH) \tag{1}$$

where $\ln(CD)$ and $\ln(DBH)$ are natural logarithms of CD and DBH. Regression coefficients are $b_0$ and $b_1$. However, it took so much time to measure CD for each tree within a plot that it seemed impossible that a reasonable number of plots can be made with resources available. After the first sampling plot, only 16 individuals uniformly distributed within the range of DBH of the plot were selected to measure the crown diameter. A laptop was used to evaluate the relationship immediately in the field to see if more individuals were needed. This sampling scheme worked well for mono-species Loblolly pine stands. However, when the sampling plot was made in a hardwood stand, it was difficult to get a strong allometric relationship between DBH and CD because the allometry varies significantly among species. The sampling scheme was adjusted to select individuals across the diameter range for major species. At the end of the fieldwork, we pooled all the tree crown measurements from all plots by species. The allometric relationship was rebuilt on a species-specific basis. The tree crown sizes for the individuals that were not measured in the field were then calculated using equation (1) by species. After CD

was calculated for each individual within a plot, the mean crown diameter of the plot was calculated as

$$\overline{CD} = \sqrt{\frac{\sum_{i=1}^{n} CD_i^2}{n}} \tag{2}$$

where $\overline{CD}$ is the mean crown diameter of the plot, and $n$ is the number of trees within the plot. $CD_i$ is the individual tree crown diameter within the stand.

### 2.3 *Image semivariograms*

Optical remotely sensed imagery is essentially a record of reflected electromagnetic radiation (EMR) from the sun within the instantaneous field of view (IFOV) over a continuous landscape. The reflected EMR is the result of the interaction between incoming EMR with objects within the IFOV, carrying the footprints of objects. Each of the digital number (DN) from a remote sensing image is linked to a unique location on the ground. In fact, DNs in an image can be considered as the realization of a spatial random function: $DN_i = f(\boldsymbol{x_i})$, where $DN_i$ is the digital number for the $i$th pixel, $\boldsymbol{x}_i$ is the geographic location vector for the $i$th pixel and $f$ is the random spatial function that takes the value of $DN_i$ at the geographic location $\boldsymbol{x}_i$. Therefore, the DNs of a remotely sensed image can be treated as a spatial random variable, and the semivariogram from geostatistics can be used to study the spatial properties of the underlying scene. A semivariogram is a plot of semivariance against the lag in space, i.e. the plot of $\gamma(h)$ against $h$ in the following:

$$\gamma_f(h) = 1/2 E\left\{[f(x_i) - f(x_i + h)]^2\right\} \tag{3}$$

where $\gamma_f(\boldsymbol{h})$ is the semivariance for points that are $\boldsymbol{h}$ distance apart. The realization of the random spatial function $f$ is $f(\boldsymbol{x}_i)$ at location $\boldsymbol{x}_i$, and $f(\boldsymbol{x}_i + \boldsymbol{h})$ at another location $h$ distance away from $\boldsymbol{x}_i$. The lag is the distance $h$. The calculation of semivariance requires the assumption of intrinsic stationarity for $f$, i.e. the difference in the mean value of $f(\boldsymbol{x}_i)$ and $f(\boldsymbol{x}_i + \boldsymbol{h})$ is a function of $\boldsymbol{h}$ only. $E$ stands for expectation. A typical semivariogram is shown in figure 1, which can be characterized by the range, the sill and the nugget effect. The range, the lag at which the semivariance reaches its maximum value, reflecting the characteristic scale of the underlying scene and the sill is the maximum value of semivariance, representing the overall variance of the scene. Points that are separated by a distance greater than the range can be considered independent. The nugget effect is semivariance at $\boldsymbol{h}=0$. It is not directly measurable, but estimated by extending the curve of semivariogram to the $y$-axis in figure 1. Theoretically, semivariance should be zero at $\boldsymbol{h}=0$. In reality, the nugget effect is often greater than zero due to noise.

### 2.4 *Disc scene model*

The disc scene model is a simplified representation of a forest scene originally developed by Jupp (1999), which in turn was based on the theory by Jupp *et al.* (1988, 1989). The model assumes a scene that is composed of discs randomly distributed over an unbounded contrasting background. The discs can overlap, but the brightness value of the disc does not change in the overlapped area. Though simple, the model is very effective in understanding the relationship between scene

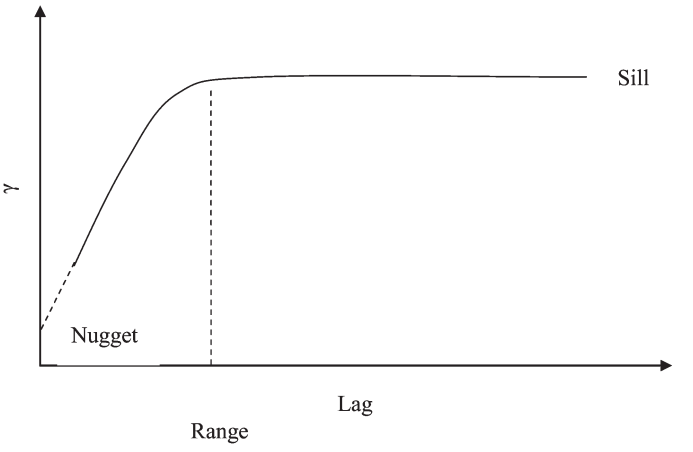


Figure 1. A typical shape of a semivariogram over a stationary scene. The characteristic parameters of a semivariogram include the sill, the range and the nugget effect. The sill is the highest value of semivariance. The range is the distance at which the semivariance reaches the sill value. Points in space with distance equal to or greater than the range can be considered independent of each other. The nugget effect is the semivariance at lag zero.

structure and the spatial characteristics of image DNs. The disc scene model is a spatially stationary scene. Therefore the semivariance in equation (3) can be simplified as

$$\gamma_f(h) = \sigma^2 - \mathrm{cov}_f(h) \tag{4}$$

where $\sigma^2$ is the variance of the scene and $\mathrm{cov}_f(h)$ is the covariance between $f(\boldsymbol{x}_i)$ and $f(\boldsymbol{x}_i + h)$. For a disc scene model, assuming the density of the disc is $\lambda$, the diameter of the disc is $D_o$ (disc area $A = \pi D_o^2/4$), the Boolean set theory (Serra 1980) indicates that the fractions of ground area that are not covered by the discs are

$$Q = e^{-\lambda A}. \tag{5}$$

Thus, the disc cover is (1 – $Q$), and the mean, variance and covariance of the brightness values in the scene are, respectively

$$S = g_B Q + g_D(1-Q), \tag{6}$$

$$\sigma^2 = (g_D - g_B)^2 Q(1-Q) \tag{7}$$

and

$$\mathrm{cov}_f(h) = (g_D - g_B)^2 Q^2 \left(e^{\lambda A T(s)} - 1\right) \tag{8}$$

where $g_D$ and $g_B$ are the brightness of the disc and background, respectively. $T(s)$ is the overlap function between two discs in space (figure 2). For two discs in space with $D_o$ in diameter, there is a fraction of overlap between the discs if the distance between the centres of the two discs, $h$, is shorter than the diameter of the disc. Thus, the fraction of overlap between the two discs in space is a function of the size of the disc and the distance between them. The overlap function defines the spatial scale of autocorrelation for the disc scene model. Thus it is critical to estimate the overlap

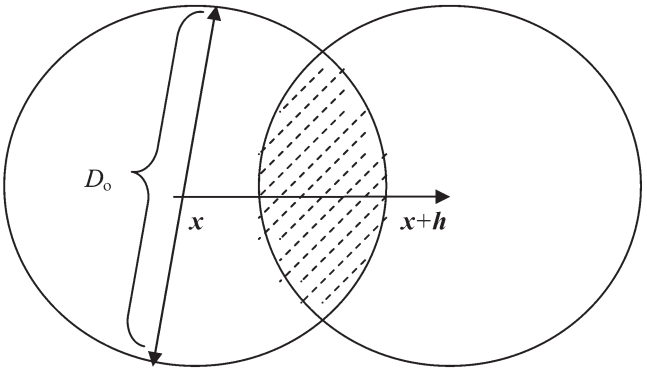


Figure 2. Overlapping of two discs in space, where $\boldsymbol{x}$ is a location vector, $D_o$ is the diameter of the disc and $\boldsymbol{h}$ is the distance between the centres of the two discs. There is an overlap when $h<D_o$ (the hashed area). There will be no overlap between the two discs in space when $\boldsymbol{h}>D_o$.

function in order to estimate the spatial covariance of equation (8). Estimating the overlap function can be significantly simplified if we define a standardized distance in space as $s=h/D_o$. Then $T(s)$ can be estimated as (Jupp *et al.* 1989)

$$T(s)=\begin{cases} 1 & h=0 \\ \frac{1}{\pi}(\theta-\sin(\theta) & h<D_o \\ 0 & h\geq D_o \end{cases} \tag{9}$$

The parameter $\theta$ is related to $s$ as $\cos(\theta/2)=s$. There is an overlap between two discs in space when $s<1$ (figure 2). When $s>1$, there would be no overlap, i.e. $T(s)=0$. Based on equation (8), $\mathrm{cov}_f(h)=0$ when $T(s)=0$, meaning two points in the disc scene are spatially independent if their distance is greater than $D_o$. Accordingly, when $s=0$, the two discs would completely overlap, i.e. $T(s)=1$. In this case, equation (8) becomes equation (7 or $\mathrm{cov}_f(h)=\sigma^2$ when $s=0$.

Equations (6)–(8) provide the theoretical basis between the structure of a disc scene and its spatial properties. However, the theory above does not apply directly to remotely sensed imagery because each DN in an optical remotely sensed imagery is a spatial integration of reflected EMR within the IFOV. The semivariogram in equation (4) is often referred to as a punctual semivariogram. The semivariogram for a remotely sensed image with a finite size of IFOV is often referred to as a regularized semivariogram. The mean of a regularized scene will not change with IFOV, i.e equation (6) remains valid for a remotely sensed image, but the variance, covariance and thus the semivariogram will change for a regularized scene. Jupp *et al.* (1988) derived the regularized semivariogram for the disc scene model as

$$\gamma_Z(h)=C_Z-\mathrm{cov}_Z(h) \tag{10}$$

where $C_Z$ is the regularized sill of the semivariogram, or variance of the regularized image, and $\mathrm{cov}_Z(h)$ is covariance of the regularized scene. According to Jupp *et al.* (1989),

$$C_Z=8\int_0^1 tT(t)\mathrm{cov}\left(D_{\mathrm{p},}\ t\right)\mathrm{d}t, \tag{11}$$

and

$$\mathrm{cov}_Z(s) = \frac{8}{\pi}\int_0^s t\Phi(t, s)\mathrm{cov}\left(D_\mathrm{p}, t\right)\mathrm{d}t \tag{12}$$

where $\mathrm{cov}(D_\mathrm{p}, t)$ is the spatial covariance of DNs with $D_\mathrm{p}$ as the diameter of IFOV. $\Phi(t, s)$ integrates the overlap function for discs over azimuth from 0 to $\pi$. In the regularized scene, the image spatial properties are determined by both the object size ($D_\mathrm{o}$) and the pixel size ($D_\mathrm{p}$). Two pixels may still be spatially correlated even if the distance between them is greater than the diameter of the object because of the pixel size effect. The theoretical characteristic scale is $D_\mathrm{p} + D_\mathrm{o}$. When $D_\mathrm{p} \gg D_\mathrm{o}$, there is no data available to estimate $\gamma_Z(h)$ in equation (10). This is true for the Li–Strahler model (Li and Strahler 1985), where only the interpixel variance and the mean of a stand were used in estimating the stand structural parameters. Recently, Jupp (1999) developed the inverse disk (INVDISK) mode in which all available spatial information, including the mean, variance and semivariograms, are used in estimating forest stand structure. This proved to be more robust theoretically because semivariograms provide additional information. The INVDISK model proved to be very effective in understanding the relationship between scene structure and image spatial properties with regard to spatial scale (Song and Woodcock 2002), but we have to convert a real remotely sensed image into a two-component image in order to use the model. This can be done for high-resolution images where the objects are significantly larger than the pixel size. However, it is difficult to do so when there are significant proportions of mixed pixels, which is the case for Ikonos imagery over a forest stand. Song and Woodcock (2003) recognized that if substituting equation (8) into equation (12), we get

$$C_Z = 8(g_\mathrm{D} - g_\mathrm{B})^2 Q^2 \int_0^1 tT(t)\left(e^{\lambda AT\left(tD_\mathrm{p}/D_\mathrm{o}\right)} - 1\right)\mathrm{d}t \tag{13}$$

where the standardized distance $s = h/D_\mathrm{p}$. This directly relates the sill of the regularized image variogram to the scene structure, the size ($D_\mathrm{o}$) and density ($\lambda$) of the objects and the contrast between the disc and the background at a given size of IFOV ($D_\mathrm{p}$). Due to the fact that the contrast between the disc and the background does not change with the size of IFOV, the ratio of the sill of regularized variogram at a second spatial resolution would be solely determined by the scene structure as

$$\frac{C_{Z1}}{C_{Z2}} = \frac{\int_0^1 tT(t)\left(e^{\lambda AT\left(tD_{\mathrm{p}1}/D_\mathrm{o}\right)} - 1\right)\mathrm{d}t}{\int_0^1 tT(t)\left(e^{\lambda AT\left(tD_{\mathrm{p}2}/D_\mathrm{o}\right)} - 1\right)\mathrm{d}t} \tag{14}$$

Equation (14) was tested with simulated images in Song and Woodcock (2003). In this study, equation (14) is tested with an Ikonos panchromatic image with an extensive set of stands whose tree crown sizes were measured near the ground. The Ikonos panchromatic image is degraded to a series of coarser spatial resolution through simple average so that the ability of equation (14) to estimate tree crown size can be evaluated at a range of spatial resolutions.

## 3. Results

### 3.1 *Tree crown size and DBH*

A total of 356 individuals were measured with DBH and CD, of which 221 were Loblolly pine. The allometric relationships between DBH and CD in equation (1) are given in table 1 based on individuals across plots. The relationship is statistically significant for all species pooled together. However, the relationship is much stronger on a species-specific basis. The $R^2$ between CD and DBH of equation (1) for most of the species is above 0.7 with exceptions of Red Oak, Sweet Gum and other miscellaneous species. Using the allometry between DBH and CD was an effective approach to expedite the sampling process in the field. Based on DBH, CD of each individual within a plot was calculated using the allometry in table 1. The mean tree crown diameter for a plot was calculated with equation (2) and is given in table 2. Table 2 indicates the plots sampled ranging from very dense young stands (e.g. Plot 11) to very old sparse stands (e.g. Plot 5). The dynamic range of the canopy structure is critical for this study. Though there are varying degrees of mixture of broadleaf and conifer species, the plots are classified into either hardwoods or conifer based on the dominant number of individuals.

### 3.2 *Image semivariograms*

Due to the stationarity assumption in equation (4), the geostatistical analysis was performed on a stand basis. It was assumed that the canopy structure derived from the sampling plot made in the middle of each stand was representative of the stand. Each of the stands is clipped from the 1 m panchromatic Ikonos image. Figure 3(*a*) shows the semivariograms for a couple of conifer forests at different spatial resolutions. The range of the variogram for the stand with bigger trees is larger than that for the stand with smaller trees. Despite the difference in tree crown size, the sills of the semivariograms for the stands are quite close at 1 m spatial resolution because the stands have quite similar canopy coverage. Based on the theory of disc scene model, i.e. equation (7), the image should have the same variance of brightness values with the same disc cover at the punctual scale regardless of disc size. Therefore, it is not surprising to see that the sills of the semivariograms are quite similar at 1 m spatial resolution. As the spatial resolution changes from 1 m to 2 m, the difference in the sill for the stands is much bigger. Similar patterns of change in

Table 1. Species-specific allometry between diameter at breast height (DBH) and tree crown diameter (CD): $\ln(CD)=b_0+b_1 \ln(DBH)$. The data were collected in the Duke Forest and its surrounding areas in the field during late spring and early summer of 2005.

| Species | $b_0$ | $b_1$ | $R^2$ | $n$ |
|---|---|---|---|---|
| All | −0.0435 | 0.06798 | 0.5034 | 238 |
| Loblolly Pine | −1.1013 | 1.0201 | 0.7673 | 103 |
| Shortleaf Pine | −0.5554 | 0.9123 | 0.8239 | 15 |
| Hickory | 0.0707 | 0.8617 | 0.8098 | 7 |
| Red Maple | 0.2572 | 0.7841 | 0.7361 | 20 |
| Sweet Gum | 0.0661 | 0.7168 | 0.5454 | 28 |
| Tulip Popular | 0.1720 | 0.6296 | 0.8348 | 29 |
| Red Oak | 0.2335 | 0.7056 | 0.5643 | 8 |
| White Oak | −0.0438 | 0.8185 | 0.8133 | 15 |
| Others | 0.4882 | 0.6028 | 0.5846 | 13 |

Table 2. Canopy structure for each sampling plot. The mixture of conifer and hardwood for the individuals in each plot is characterized by the percent basal area conifer. The average size of the individuals is indicated by the quadratic mean of diameter at breast height (DBH).

| Plot number | Basal area conifer (%) | Plot diameter (m) | Stem density (trees/ha) | Quadratic mean DBH (cm) | Plot LAI | Mean CD (m) |
|---|---|---|---|---|---|---|
| 1 | 86.7 | 30 | 1995 | 17.56 | 5.12 | 3.21 |
| 2 | 80.9 | 30 | 806 | 25.78 | 8.28 | 4.86 |
| 3 | 92.0 | 30 | 2080 | 16.93 | 4.09 | 2.92 |
| 4 | 92.2 | 30 | 1811 | 18.22 | 3.98 | 2.99 |
| 5 | 17.2 | 30 | 566 | 28.50 | 8.32 | 6.33 |
| 6 | 98.1 | 30 | 1500 | 19.90 | 3.63 | 2.94 |
| 7 | 83.3 | 30 | 1712 | 18.59 | 6.48 | 3.22 |
| 8 | 9.8 | 30 | 608 | 24.96 | 8.71 | 5.99 |
| 9 | 0.0 | 30 | 3240 | 9.82 | 7.18 | 3.13 |
| 10 | 38.5 | 30 | 905 | 23.46 | 9.67 | 5.41 |
| 11 | 26.9 | 15 | 8715 | 6.04 | 5.67 | 1.83 |
| 12 | 0.0 | 40 | 668 | 21.24 | 6.23 | 4.98 |
| 13 | 51.9 | 30 | 920 | 23.95 | 9.17 | 5.01 |
| 14 | 10.5 | 40 | 613 | 28.61 | 11.72 | 5.01 |
| 15 | 100.0 | 20 | 1974 | 15.42 | 3.66 | 2.88 |
| 16 | 88.6 | 30 | 1160 | 23.35 | 7.25 | 4.61 |
| 17 | 87.6 | 30 | 1075 | 22.73 | 5.51 | 4.38 |
| 18 | 76.1 | 30 | 1174 | 19.21 | 6.20 | 5.35 |
| 19 | 92.5 | 30 | 495 | 26.69 | 3.33 | 5.50 |
| 20 | 87.8 | 30 | 1146 | 21.37 | 4.74 | 4.06 |
| 21 | 86.3 | 30 | 1203 | 20.57 | 4.96 | 3.41 |

CD, crown diameter; and LAI, leaf area index.

the sills of the semivariograms are observed for the hardwood stands as shown in figure 3(*b*).

### 3.3 *Tree crown size and image spatial properties*

The relationship between tree crown size and the image spatial properties was examined separately for conifer and hardwood stands with single resolution and multiple resolution images. Table 3 shows that relationship between mean CD and image variance at a single spatial resolution. The relationships are significant with *p*-values less than 0.05 for images at all spatial resolutions for conifer stands except at 1 m spatial resolution. It is interesting to note that the highest $R^2$ value is not at the highest spatial resolution, but at 4 m spatial resolution. This phenomenon is similar to what Woodcock and Strahler (1987) found for the relationship between image texture at $3 \times 3$ windows and the object size. However, the relationship is not significant for the hardwood stands at any spatial resolution. This may be due to the fact that the canopy structure in the hardwood stands is more continuous than the conifer stands seen from above. It is difficult to isolate individual crown even with human eyes on the ground. The boundaries of tree crowns are much less clearly defined in the image for hardwood stands than for conifer stands.

The theoretical basis for the relationship between tree crown size and the spatial properties of multiple resolution images is equation (14). Table 4 shows the relationship between tree crown size and the ratio of image variances at two spatial resolutions. The maximum $R^2$ increased for both conifer and hardwood stands. For

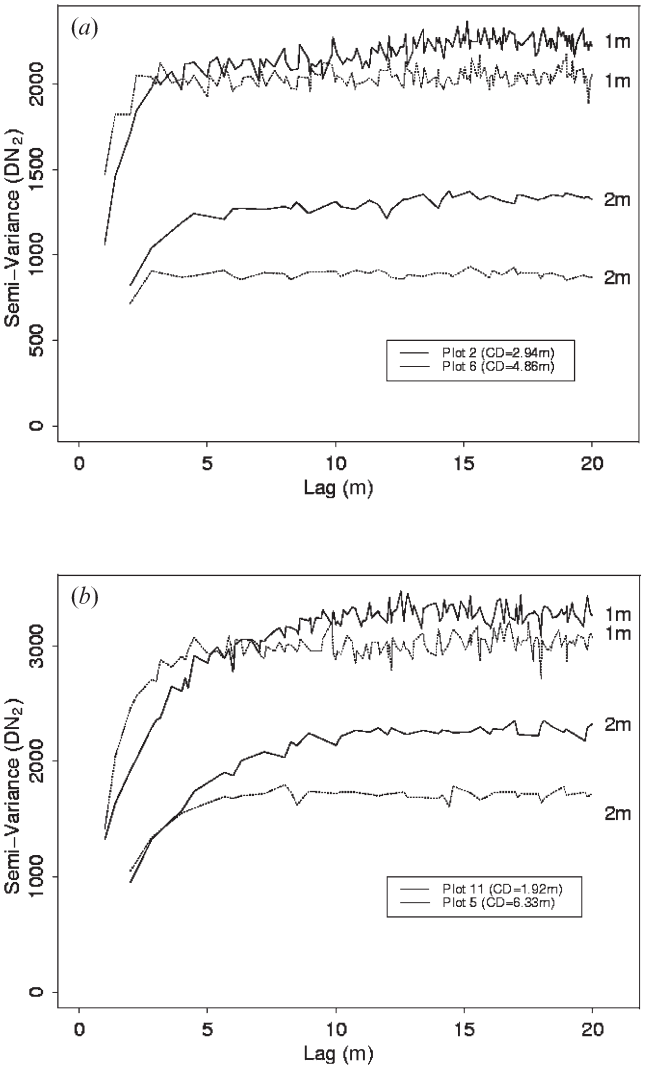


Figure 3. Semivariograms at two spatial resolutions for two stands with contrasting crown sizes for conifers (*a*) and hardwoods (*b*).

conifer stands, the maximum $R^2$ is 0.7282 with the ratio of image variances at 2 m spatial resolution to that at 3 m spatial resolution. The $R^2$ decreases rapidly after reaching the maximum value.

In order to better understand the relationship between tree crown size and the ratio of image variances at different spatial resolutions, the regularized sill of image variance was generated using equation (13) with different sizes of discs and then the ratio of the sills, as shown in figure 4, were calculated. The ratio increases with pixel size when the pixel size is smaller than the object, and peaks around the spatial resolution equivalent to the object size. After the peak, the ratio decreases approaching 1. However, the rate of decrease and increase in the ratio is strongly related to object size. The optimal spatial resolution is at the one at which the vertical distances between different object sizes on the vertical axis in figure 4 maximize. The rapid converging of the lines in figure 4 explains why the $R^2$

Table 3. Relationship between tree crown size and image variance of single resolution images: $CD=b_0+b_1C_Z$, where $CD$ is crown diameter (m) and $C_Z$ is the regularized sill. The relationship was examined for conifers and hardwoods separately at six spatial resolutions.

| Resolution | $R^2$ | $p$-value |
|---|---|---|
| Conifers | | |
| 1 m × 1 m | 0.2880 | 0.0586 |
| 2 m × 2 m | 0.5175 | 0.0056 |
| 3 m × 3 m | 0.6127 | 0.0016 |
| 4 m × 4 m | 0.6214 | 0.0014 |
| 5 m × 5 m | 0.5689 | 0.0029 |
| 6 m × 6 m | 0.5735 | 0.0037 |
| Hardwoods | | |
| 1 m × 1 m | 0.0930 | 0.4627 |
| 2 m × 2 m | 0.1569 | 0.3313 |
| 3 m × 3 m | 0.2134 | 0.2492 |
| 4 m × 4 m | 0.2227 | 0.2377 |
| 5 m × 5 m | 0.2212 | 0.2396 |
| 6 m × 6 m | 0.1327 | 0.3749 |

decreased very fast for the conifer stands in table 4. For hardwoods, the $R^2$ decreases much slower as the cell size increases. The slow decrease is an indication of the large object size, reflecting continuous nature of the canopy for hardwoods.

As a comparison to the ratio of image variance, the relationships between the difference of image variances at multiple spatial resolutions and the tree crown size are examined (figure 5). The maximum $R^2$ value is lower than that from the ratios. As equation (14) indicates, the ratio of the image variance removed the effect of contrast between the object and the background. However, the spatial variation of the brightness contrast between the object and background cannot be removed in the difference. The spatial variation of the contrast may have contributed to the lower maximum $R^2$ value in figure 5.

Table 4. Relationship between tree crown size and image variance of multiple resolution image: $CD=b_0+b_1C_{Zi}/C_{Zj}$, where $CD$ is crown diameter (m) and $C_{Zi}/C_{Zj}$ is the ratio of the regularized sills at spatial resolutions $i$ and $j$. The relationship was examined for conifers and hardwoods separately.

| Resolution | $R^2$ | $p$-value |
|---|---|---|
| Conifers | | |
| $C_{Z1}/C_{Z2}$ | 0.6175 | 0.0015 |
| $C_{Z2}/C_{Z3}$ | 0.7282 | 0.0002 |
| $C_{Z3}/C_{Z4}$ | 0.3601 | 0.0301 |
| $C_{Z4}/C_{Z5}$ | 0.0535 | 0.4473 |
| $C_{Z5}/C_{Z6}$ | 0.0513 | 0.4566 |
| $C_{Z6}/C_{Z7}$ | 0.0511 | 0.4579 |
| Hardwoods | | |
| $C_{Z1}/C_{Z2}$ | 0.3053 | 0.1555 |
| $C_{Z2}/C_{Z3}$ | 0.4723 | 0.0597 |
| $C_{Z3}/C_{Z4}$ | 0.3802 | 0.1035 |
| $C_{Z4}/C_{Z5}$ | 0.3467 | 0.1246 |
| $C_{Z5}/C_{Z6}$ | 0.3206 | 0.1434 |
| $C_{Z6}/C_{Z7}$ | 0.0868 | 0.4787 |

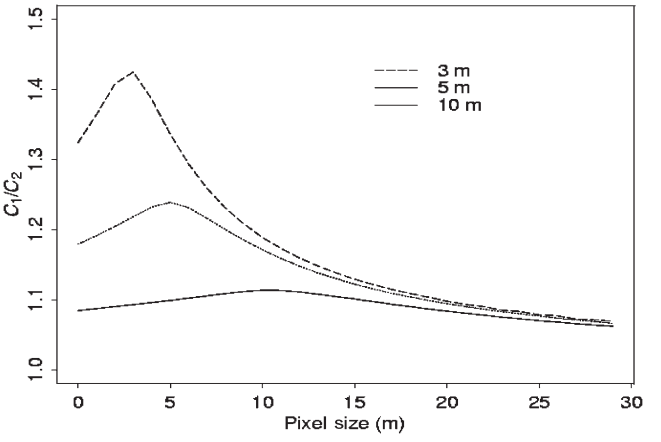


Figure 4. Simulated ratio of sills at two spatial resolutions as a function of object size. The ratio best relates to object size in the spatial resolution where the vertical distances among the lines maximize. The lines quickly converge and approach an asymptote at 1, indicating the pixel size is much bigger with respect to the object size and regularization causes little change in image variance.

Figure 5(*a*) shows that the image variance decreases less for images containing larger tree crowns than for those with smaller trees from 1 m to 2 m spatial resolution. This confirms the finding in an early study that the rate of decrease in image variance during regularization is diagnostic of object size (Song and Woodcock 2003). However, the relationship is reversed as the spatial resolution of the image is further coarsened, i.e. the image variance decreases more for a scene containing larger trees than that for a scene containing smaller ones. The seemingly contradictory relationships are in fact the result of the interactions of object size and scales of regularization. According to equation (7), image variance at punctual scale is determined by the contrast between the objects and the background and the coverage of the object, i.e. image variance is independent of object size at punctual scale. The object size becomes important during the regularization process. Due to spatial averaging, the variances of a regularized image become increasingly smaller as the cell size increases. The smaller the object the image contains, the faster the rate of decrease in the image variance. However, when the cell size is big enough with respect to the object size, there will not be much variance in the image, thus the change of variance during regularization will be small. This happens sooner for images with smaller trees. Therefore, we see a positive relationship between the decreases of image variance and object size in figure 5(*c*)–(*f*). But these relationships are not as strong as that depicted in figure 5(*a*) because the overall information content is lower.

Another important difference between using the ratio of image variances and the difference of image variances is figure 5(*b*) which has the lowest $R^2$ in figure 5. Figure 5(*b*) shows a poor relationship between tree crown size and the difference of image variances at 2 m and 3 m spatial resolutions. However, table 4 shows it is at the exact same two spatial resolutions that the ratio of the image variances has the highest $R^2$ in its relationship with the tree crown size. In order to understand the difference, the variances for the twelve conifer stands are plotted in figure 6 as they are progressively regularized with larger cells. The variances for the images of all 12 conifer stands decrease as the cell size increases. The lines between the spatial

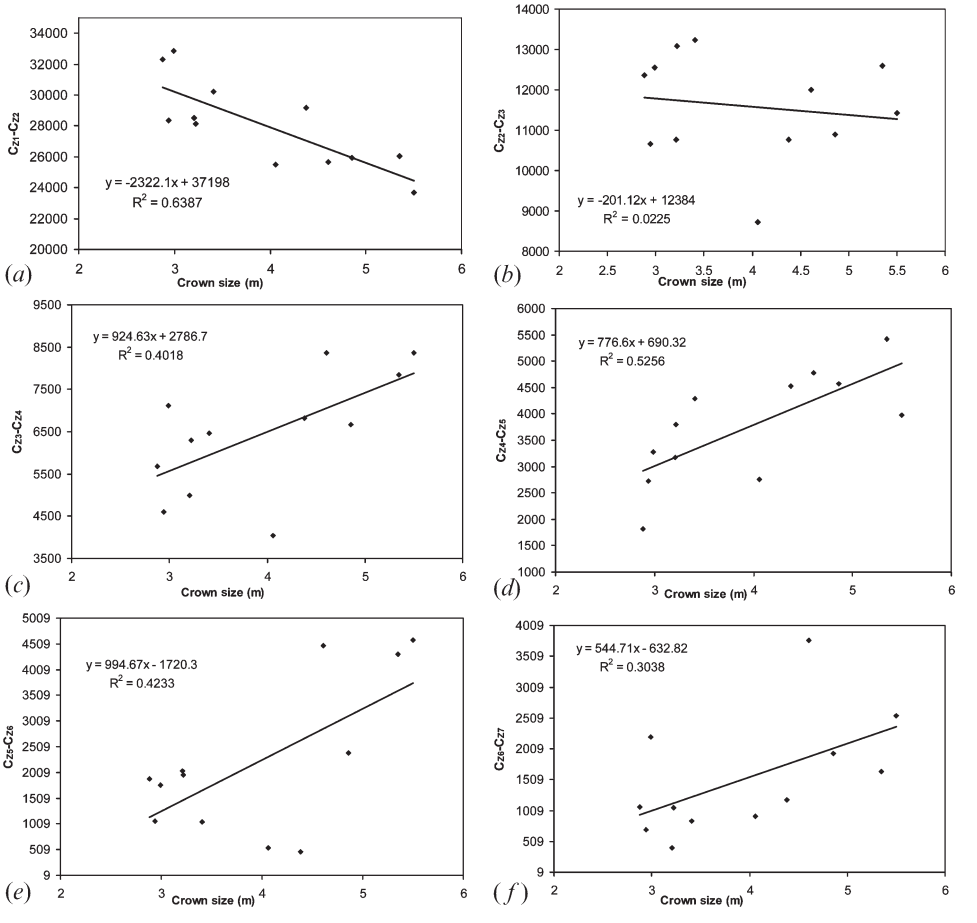


Figure 5. The ability of difference of image variance from two spatial resolutions in estimating tree crown size. At finer spatial resolutions, the decrease in image variance is inversely related to tree size. However, as the pixel becomes larger, the relationship is reversed at coarser spatial resolutions.

resolutions at 2 m and 3 m are very well separated and almost parallel to each other. However, the differences in image variances at these spatial resolutions among these stands are quite similar, which leads to the low $R^2$ in figure 5(*b*). The unique information for the stands are maintained and even enhanced in the ratios between image variances at the two spatial resolutions. This further confirms that the ratio of image variances at multiple resolutions is more advantageous than the difference in image variances in extracting tree crown size.

## 4. Discussion

Given the importance of canopy structure in forest ecosystem gaseous and energy exchanges with the atmosphere (Chen and Coughenour 1994, Betts *et al.* 1997, Song and Band 2004), the value of extracting tree crown size on a stand basis from high spatial resolution imagery is significant. This provides the possibility to include these important, yet generally missing biophysical parameters into ecosystem models at a regional scale helping to enhance our understanding of the relationship between

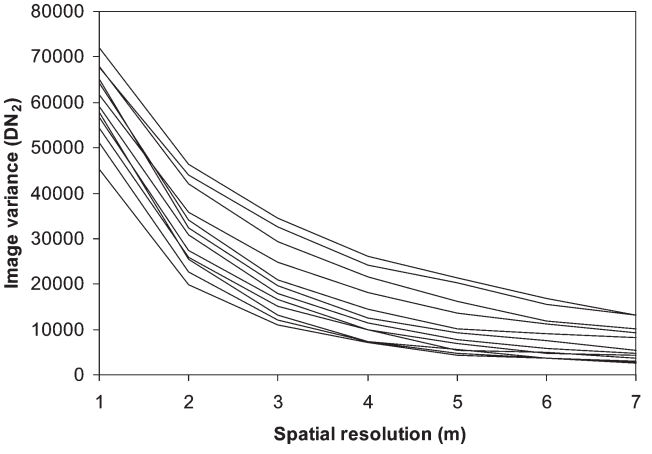


Figure 6. Change of image variance as a function of pixel size for the 12 conifer stands in this study. The stands are best distinguished between 2 m and 3 m spatial resolutions, which is the spatial resolution where the ratio of the image variances best correlates to tree crown size.

ecosystem structures and its functions. However, the approach developed in this study is effective only for conifer stands. It remains a challenge for extracting tree crown sizes for hardwood stands. If the human eyes have difficulty in separating the tree crowns on the ground for hardwood stands, it is hardly possible to derive the parameter with optical remotely sensed imagery from space regardless of the spatial resolution. An alternative technology might be lidar. Lidar imagery provides accurate measurements of canopy heights and canopy volumes (Lefsky *et al.* 1999). There is potential that the tree crown size may be derived from lidar imagery indirectly.

Obtaining canopy structure from remotely sensed imagery has been a major effort by remote sensing scientists (Li and Strahler 1985, Cohen and Spies 1992, Hall *et al.* 1995, Peddle *et al.* 1999, Asner *et al.* 2002, Clark *et al.* 2004b). According to Strahler *et al.* (1986), earlier work on this subject can be characterized into either L-resolution case, which is primarily based on Landsat TM imagery with the pixel size substantially bigger than tree crown size, or H-resolution case, which is based on airborne imagery with a pixel size ranging from several centimetres to a metre. There is very limited success in deriving detailed forest structural parameters from the L-resolution case. A number of automatic algorithms have been developed in the literature in delineating tree crowns in the H-resolution case (Chen *et al.* 1993, Pollock 1996, Brandtberg and Walter 1998, Wulder *et al.* 2000, Culvenor 2002). However, the automatic tree crown identification algorithms suffer from two major drawbacks: (i) they cannot separate overlapping tree crowns, which are ubiquitous in natural forest stands; and (ii) computation is very intensive, thus it cannot be operationalized over a sizable area. With the recent availability of remotely sensed imagery from space at sub-metre spatial resolution, the Ikonos/QuickBird imagery was found to be highly valuable in extracting forest canopy structure (Asner *et al.* 2002, Clark *et al.* 2004b). But we lack an automated approach to take advantage of, particularly with regards to tree crown size at regional scale. The ability to extract tree crown sizes from the ratio of image variances at two spatial resolutions is critical to operationalize the approach. The ratio removed the effect of the contrast between the object and the background, which can vary significantly over the landscape and can be a major uncertainty factor. In addition, this approach is not

limited by the drawbacks that the automatic tree crown delineation approaches suffer. First, the approach allows overlap of tree crowns. Second, it is computationally much more efficient, particularly if a regional stand map exists. Finally, at 1 m spatial resolution, the automatic tree crown delineation algorithms may only work for very large trees. However, the approach developed in this paper only provides an ensemble mean tree crown size for each stand, no individual tree crown size is available as in the automatic tree crown delineation algorithms. Therefore, when individual tree crown sizes are needed, this approach is not applicable. Moreover, one has to have a significant number ground truth data before applying this approach to a landscape scale. The ground truth data may not be needed on a scene-by-scene basis as the ratio of the image variances at two spatial resolutions removed the influence of the brightness value of the pixels. This implies that the relationship established in one scene may be applicable to Ikonos images collected at other scenes. This was part of the original objectives in this study. In addition to the stands used in this study, the author also collected a similar number of sampling plots in Vinton Furnace Experimental Forest, Ohio during summer 2005. Unfortunately, no cloud-free Ikonos images were collected during that period despite multiple attempts by Space-imaging. This effort is now pending depending on image acquisition from Ikonos in summer of 2006.

Obtaining canopy structures from high spatial resolution optical imagery is much cheaper and easier to implement than the current efforts using lidar imagery. Ikonos images can now be obtained anywhere around the globe as long as the weather conditions allow. In addition, obtaining tree crown sizes from high-resolution optical images can add significant synergistic values to lidar images. Lidar images primarily provide canopy height information (Lefsky *et al.* 1999, Weishampel *et al.* 2000, Naesset and Okland 2002), they do not provide crown size information. Thus estimating aboveground biomass from lidar images is primarily based on canopy height (Drake *et al.* 2003, Lefsky *et al.* 2005). Adding crown size information can significantly improve the accuracy of the biomass estimation (Popescu *et al.* 2003).

## 5. Conclusions

This study investigated the potential of extracting tree crown sizes from high-resolution optical imagery. There exists a much stronger relationship of tree crown size with image spatial property at multiple spatial resolutions than that at a single spatial resolution. It is noted that the strongest relationship between tree crown size and image spatial properties does not occur at the highest spatial resolution. There appears to be an optimal spatial resolution where the image spatial properties best correlate with tree crown size. The study also found that the ratio of image variances has a stronger relationship with tree crown size than the difference around the optimal spatial resolution. However, the relationship between image spatial properties and tree crown size is much weaker for hardwoods than it is for conifers due to its continuous nature of canopy structure. The findings in this study have significant implications for ecosystem modelling, forest management and inventories, and other related studies that use high-resolution optical imagery.

**Acknowledgement**

The author wishes to thank Andrea Nifong, Elizabeth Ward, Bo Xiao and students in Geog 178 class in spring of 2005 at University of North Carolina at Chapel Hill for their

participation in field data collection. This work was supported by NSF grant 0351430 and USDA Forest Service Agenda 2020 program. The manuscript was completed while the author was a Charles Bullard Fellow in Forest Research at Harvard Forest, Harvard University between the period 1 September 2005 to 31 May 2006.

## References

ALVES, L.F. and SANTOS, F.A.M., 2002, Tree allometry and crown shape of four tree species in Atlantic rain forest, southeast, Brazil. *Journal of Tropical Ecology*, **18**, pp. 245–260.

ASNER, G.P., PALACE, M., KELLER, M., PEREIRA, R., SILVA, J.N.M. and CLARK, D.A., 2002, Estimating canopy structure in an Amazon Forest from laser range finder and IKONOS satellite observations. *Biotropica*, **34**, pp. 483–492.

BECHTOLD, W.A., 2004, Largest-crown-width prediction models for 53 species in the western United States. *Western Journal of Applied Forestry*, **19**, pp. 245–251.

BETTS, R.A., COX, P.M., LEE, S.E. and WOODWARD, F.I., 1997, Contrasting physiological and structural vegetation feed backs in climate change simulations. *Nature*, **387**, pp. 796–799.

BRANDTBERG, T. and WALTER, F., 1998, Automated delineation of individual tree crowns in high spatial resolution aerial images by multiple-scale analysis. *Machine Vision and Applications*, **11**, pp. 64–73.

CHEN, D.X. and COUGHENOUR, M.B., 1994, GEMTM – A general model for energy and mass transfer of land surfaces and its application at the FIFE sites. *Agricultural and Forest Meteorology*, **68**, pp. 145–171.

CHEN, R., WOODCOCK, C.E., STRAHLER, A.H. and JUPP, D.L.B., 1993, Nonlinear estimation of scene parameters from digital images using zero-hit run-length statistics. *IEEE Transactions on Geoscience and Remote Sensing*, **31**, pp. 735–746.

CLARK, D.B., CASTRO, C.S., ALVARADO, L.D.A. and READ, J.M., 2004a, Quantifying mortality of tropical rain forest trees using high-spatial-resolution satellite data. *Ecology Letters*, **7**, pp. 52–59.

CLARK, D.B., READ, J.M., CLARK, M.L., CRUZE, A.M., DOTTI, M.F. and CLARK, D.A., 2004b, Application of 1-M and 4-M resolution satellite data to ecological studies of tropical rain forests. *Ecological Applications*, **14**, pp. 61–74.

COHEN, W.B. and SPIES, T.A., 1990, Semivariograms of digital imagery for analysis of conifer canopy structure. *Remote Sensing of Environment*, **34**, pp. 167–178.

COHEN, W.B. and SPIES, T.A., 1992, Estimating structural attributes of Douglas-fir western Hemlock forest stands from Landsat and spot imagery. *Remote Sensing of Environment*, **41**, pp. 1–17.

CULVENOR, D.S., 2002, TIDA: an algorithm for the delineation of tree crowns in high spatial resolution remotely sensed imagery. *Computers and Geosciences*, **28**, pp. 33–44.

DRAKE, J.B., KNOX, R.G., DUBAYAH, R.O., CLARK, D.B., CONDIT, R., BLAIR, J.B. and HOFTON, M., 2003, Above-ground biomass estimation in closed canopy neotropical forests using lidar remote sensing: factors affecting the generality of relationships. *Global Ecology and Biogeography*, **12**, pp. 147–159.

FRANKLIN, J. and STRAHLER, A.H., 1988, Invertible canopy reflectance modeling of vegetation structure in semi-arid woodland. *IEEE Transactions on Geoscience and Remote Sensing*, **26**, pp. 809–825.

FRANKLIN, S.E., WULDER, M.A. and GERYLO, G.R., 2001, Texture analysis of IKONOS panchromatic data for Douglas-fir forest age class separability in British Columbia. *International Journal of Remote Sensing*, **22**, pp. 2627–2632.

HALL, F.G., SHIMABUKURO, Y. and HUEMMRICH, K.F., 1995, Remote sensing of forest biophysical structure using mixture decomposition and geometric reflectance models. *Ecological Applications*, **5**, pp. 993–1013.

HEMERY, G.E., SAVILL, P.S. and PRYOR, S.N., 2005, Applications of the crown diameter-stem diameter relationship for different species of broadleaved trees. *Forest Ecology and Management*, **215**, pp. 285–294.

HURTT, G., XIAO, X.M., KELLER, M., PALACE, M., ASNER, G.P., BRASWELL, R., BRONDIZIO, E.S., CARDOSO, M., CARLVAHO, C.J.R., FEARON, M.G., GUILD, L., HAGEN, S., HETRICK, S., MOORE, B., NOBRE, C., READ, J.M., SA, T., SCHLOSS, A., VOURLITIS, G. and WICKEL, A.J., 2003, IKONOS imagery for the large scale biosphere–atmosphere experiment in Amazonia (LBA). *Remote Sensing of Environment*, **88**, pp. 111–127.

JUPP, D.L.B., 1999, INVDISK – Inversion of disk model 'images' using mean, variance and variogram data. Personal communication.

JUPP, D.L.B., STRAHLER, A.H. and WOODCOCK, C.E., 1988, Autocorrelation and regularization in digital images. I. Basic theory. *IEEE Transactions on Geoscience and Remote Sensing*, **26**, pp. 463–473.

JUPP, D.L.B., STRAHLER, A.H. and WOODCOCK, C.E., 1989, Autocorrelation and regularization in digital images. II. Simple image models. *IEEE Transactions on Geoscience and Remote Sensing*, **27**, pp. 247–258.

KUCHARIK, C.J., NORMAN, J.M. and GOWER, S.T., 1999, Characterization of radiation regimes in nonrandom forest canopies: theory, measurements, and a simplified modeling approach. *Tree Physiology*, **19**, pp. 695–706.

LEFSKY, M.A., COHEN, W.B., ACKER, S.A., PARKER, G.G., SPIES, T.A. and HARDING, D.J., 1999, Lidar remote sensing of the canopy structure and biophysical properties of Douglas-fir western hemlock forests. *Remote Sensing of Environment*, **70**, pp. 339–361.

LEFSKY, M.A., HARDING, D.J., KELLER, M., COHEN, W.B., CARABAJAL, C.C., ESPIRITO-SANTO, F.D., HUNTER, M.O. and DE OLIVEIRA JR., R., 2005, Estimates of forest canopy height and aboveground biomass using ICESat. *Geophysical Research Letters*, **32**, art. no. L22S02.

LI, X. and STRAHLER, A.H., 1985, Geometric-optical modeling of a conifer forest canopy. *IEEE Transactions on Geoscience and Remote Sensing*, **23**, pp. 705–721.

LI, X. and STRAHLER, A.H., 1992, Geometric-optical bidirectional reflectance modeling of the discrete crown vegetation canopy: effect of crown shape and mutual shadowing. *IEEE Transactions on Geoscience and Remote Sensing*, **30**, pp. 276–292.

LI, X., STRAHLER, A.H. and WOODCOCK, C.E., 1995, A hybrid geometric optical-radiative transfer approach for modeling albedo and directional reflectance of discontinuous canopies. *IEEE Transactions on Geoscience and Remote Sensing*, **33**, pp. 466–480.

NAESSET, E. and OKLAND, T., 2002, Estimating tree height and tree crown properties using airborne scanning laser in a boreal nature reserve. *Remote Sensing of Environment*, **79**, pp. 105–115.

NI, W., LI, X., WOODCOCK, C.E., BOUJEAN, J. and DAVIS, R.E., 1997, Transmission of solar radiation in boreal conifer forests: measurements and models. *Journal of Geophysical Research*, **102**, pp. 29 555–29 566.

OREN, R., ELLSWORTH, D.S., JOHNSEN, K.H., PHILLIPS, N., EWERS, B., MAIER, C., SCHAFER, K.V.R., MCCARTHY, H., HENDREY, G., MCNULTY, S.G. and KATUL, G.G., 2001, Soil fertility limits carbon sequestration by forest ecosystems in a $CO_2$-enriched atmosphere. *Nature*, **411**, pp. 469–472.

PEDDLE, D.R., HALL, F.G. and LEDREW, E.F., 1999, Spectral mixture analysis and Geometric-Optical reflectance modeling of boreal forest biophysical structure. *Remote Sensing of Environment*, **67**, pp. 288–297.

POLLOCK, R.J., 1996, The automatic recognition of individual trees in aerial images of forests based on a synthetic tree crown image model. PhD thesis, University of British Columbia, Vancouver, Canada.

POPESCU, S.C., WYNNE, R.H., NELSON, R.F. and MOREIRA, M.P., 2003, Measuring individual tree crown diameter with Lidar and assessing its influence on estimating forest volume and biomass. *Canadian Journal of Remote Sensing*, **29**, pp. 564–577.

READ, J.M., CLARK, D.B., VENTICINQUE, E.M. and MOREIRA, M.P., 2003, Application of merged 1-m and 4-m resolution satellite data to research and management in tropical forests. *Journal of Applied Ecology*, **40**, pp. 592–600.

SCHAFER, K.V.R., OREN, R., LAI, C. and KATUL, G.G., 2002, Hydrologic balance in an intact temperate forest ecosystem under ambient and elevated atmospheric $CO_2$ concentration. *Global Change Biology*, **8**, pp. 895–911.

SERRA, J., 1980, The Boolean mode and random sets. *Computers Graphics and Image Processing*, **12**, pp. 99–126.

SHINOZAKI, K., YODA, K., HOZUMI, K. and KIRA, T., 1964, A quantitative theory of plant form – the pipe model theory. I. Basis analysis. *Japanese Journal of Ecology*, **14**, pp. 97–105.

SONG, C. and BAND, L.E., 2004, MVP: a model to simulate the spatial patterns of photosynthetically active radiation under discrete forest canopies. *Canadian Journal of Forest Research*, **34**, pp. 1192–1203.

SONG, C. and WOODCOCK, C.E., 2002, The spatial manifestation of forest succession in optical imagery: the potential of multiresolution imagery. *Remote Sensing of Environment*, **82**, pp. 272–285.

SONG, C. and WOODCOCK, C.E., 2003, Estimating tree crown size from multiresolution remotely sensed imagery. *Photogrammetric Engineering and Remote Sensing*, **69**, pp. 1263–1270.

ST-ONGE, B.A. and CAVAYAS, F., 1995, Automated forest structure mapping from high resolution imagery based on directional semivariogram estimates. *Remote Sensing of Environment*, **61**, pp. 82–95.

ST-ONGE, B.A. and CAVAYAS, F., 1997, Estimating forest stand structure from high resolution imagery using the directional variogram. *International Journal of Remote Sensing*, **16**, pp. 1999–2021.

STRAHLER, A.H., WOODCOCK, C.E. and SMITH, J.A., 1986, On the nature of models in remote sensing. *Remote Sensing of Environment*, **20**, pp. 121–139.

TREITZ, P. and HOWARTH, P., 2000, High spatial resolution remote sensing data for forest ecosystem classification: an examination of spatial scale. *Remote Sensing of Environment*, **72**, pp. 268–289.

WALLACE, C.S.A. and MARSH, S.E., 2005, Characterizing the spatial structure of endangered species habitat using geostatistical analysis of IKONOS imagery. *International Journal of Remote Sensing*, **26**, pp. 2607–2629.

WANG, L., SOUSA, W.P., GONG, P. and BIGING, G.S., 2004, Comparison of IKONOS and QuickBird images for mapping mangrove species on the Caribbean coast of Panama. *Remote Sensing of Environment*, **91**, pp. 432–440.

WEISHAMPEL, J.F., BLAIR, J.B., KNOX, R.G., DUBAYAH, R. and CLARK, D.B., 2000, Volumetric lidar return patterns from an old-growth tropical rainforest canopy. *International Journal of Remote Sensing*, **21**, pp. 409–415.

WHITE, J.C., WULDER, M.A., BROOKS, D., REICH, R. and WHEATE, R.D., 2004, Mapping mountain pine beetle infestation with high spatial resolution satellite imagery. *Forestry Chronicle*, **80**, pp. 743–745.

WOODCOCK, C.E. and STRAHLER, A.H., 1987, The factor of scale in remote sensing. *Remote Sensing of Environment*, **21**, pp. 311–332.

WOODCOCK, C.E., COLLINS, J.B., GOPAL, S., JAKABHAZY, V.D., LI, X. and MACOMBER, S.A., *et al.* 1994, Mapping forest vegetation using Landsat TM imagery and a canopy reflectance model. *Remote Sensing of Environment*, **50**, pp. 240–254.

WOODCOCK, C.E., COLLINS, J.B., JAKABHAZY, V.D., LI, X., MACOMBER, S.A. and WU, Y., 1997, Inversion of the Li–Strahler canopy reflectance model for mapping forest structure. *IEEE Transactions on Geoscience and Remote Sensing*, **35**, pp. 405–414.

WOODCOCK, C.E., STRAHLER, A.H. and JUPP, D.L.B., 1988a, The use of variograms in remote sensing: I. scene models and simulated images. *Remote Sensing of Environment*, **25**, pp. 323–348.

WOODCOCK, C.E., STRAHLER, A.H. and JUPP, D.L.B., 1988b, The use of variograms in remote sensing: II. real digital images. *Remote Sensing of Environment*, **25**, pp. 349–379.

WU, Y. and STRAHLER, A.H., 1993, Remote estimation of crown size, stand density and foliage biomass on the Oregon transect. *Ecological Applications*, **4**, pp. 299–312.

WULDER, M.A., HALL, R.J. and COOPS, N.C., *et al.* 2004, High spatial resolution remotely sensed data for ecosystem characterization. *Bioscience*, **54**, pp. 511–521.

WULDER, M., NIEMANN, K.O. and GOODENOUGH, D.G., 2000, Local maximum filtering for the extraction of tree locations and basal area from high spatial resolution imagery. *Remote Sensing Of Environment*, **73**, pp. 103–114.